Biophysical Journal
Article

Biophysical Society

Interplay of Platelet Contractility and Elasticity of Fibrin/Erythrocytes in Blood Clot Retraction

Valerie Tutwiler,[1,2] Hailong Wang,[3,4] Rustem I. Litvinov,[1] John W. Weisel,[1] and Vivek B. Shenoy[4,*]
[1]Department of Cell and Developmental Biology, Perelman School of Medicine, University of Pennsylvania, Philadelphia, Pennsylvania; [2]School of Biomedical Engineering, Sciences and Health Systems, Drexel University, Philadelphia, Pennsylvania; [3]Department of Modern Mechanics, CAS Key Laboratory of Mechanical Behavior and Design of Materials, University of Science and Technology of China, Hefei, Anhui, China; and [4]Department of Materials Science and Engineering, University of Pennsylvania, Philadelphia, Pennsylvania

ABSTRACT Blood clot contraction (retraction) is driven by platelet-generated forces propagated by the fibrin network and results in clot shrinkage and deformation of erythrocytes. To elucidate the mechanical nature of this process, we developed a model that combines an active contractile motor element with passive viscoelastic elements. Despite its importance for thrombosis and wound healing, clot contraction is poorly understood. This model predicts how clot contraction occurs due to active contractile platelets interacting with a viscoelastic material, rather than to the poroelastic nature of fibrin, and explains the observed dynamics of clot size, ultrastructure, and measured forces. Mechanically passive erythrocytes and fibrin are present in series and parallel to active contractile cells. This mechanical interplay induces compressive and tensile resistance, resulting in increased contractile force and a reduced extent of contraction in the presence of erythrocytes. This experimentally validated model provides the fundamental mechanical basis for understanding contraction of blood clots.

INTRODUCTION

The development of contractile forces by cells such as platelets, fibroblasts, endothelial cells, and smooth muscle cells is known to play important physiological roles in processes ranging from blood clot formation to wound healing and metastasis. The functionality and response of these contractile cells are often linked to their interaction with the surrounding matrix (1,2). To quantitatively assess the interplay of a viscoelastic matrix with active contractile cells, we coupled analytical and numerical methods with in vitro experiments on whole blood clots (Fig. 1). Constrained and unconstrained contraction was followed through the use of optical tracking and rheometry for samples with and without red blood cells (RBCs), which allowed for the viscoelastic component of the clot to be varied while the active contractile cells were kept constant. These experimental samples informed the development of the model by separating the relative contribution of the viscoelastic matrix from that of the active contractile cells. The model predicts the extent of contraction, which can be tested experimentally through unconstrained clot contraction studies.

Whole blood clots are composed largely of platelets, fibrin, and RBCs. Platelets are contractile cells (1) that are activated by various chemical stimuli, such as thrombin (3,4), which results in the reorganization of the platelet cytoskeleton (5). This reorganization is driven by the energy-dependent interaction of nonmuscle myosin IIa with actin and is followed by the relocation of actin filaments to the filopodia on the periphery of the platelet (5). In addition to activating platelets, thrombin converts fibrinogen to fibrin (6–9) and activates factor XIII (FXIII → FXIIIa), which catalyzes the cross-linking of fibrin (6). Cross-linking results in the stabilization of the viscoelastic fibrin network, which has many fibers originating from platelet aggregates (6–9). The activated platelets are able to generate contractile forces that are propagated through the cross-linked fibrin fibers (10,11), effectively resulting in a reduction of the clot volume (12,13). The volume reduction of the clot, or clot contraction, has been suggested to play a critical role in hemostasis (14), wound healing, and the restoration of blood flow past otherwise obstructive blood clots (15).

Although much is known about the mechanical properties of the constitutive components of clots, little is known about the dynamics of their interactions. Single contractile cells such as platelets display a force-velocity relationship that is well characterized by the Hill equation due to the

Submitted July 21, 2016, and accepted for publication January 6, 2017.
*Correspondence: vshenoy@seas.upenn.edu
Editor: Anatoly Kolomeisky.
http://dx.doi.org/10.1016/j.bpj.2017.01.005

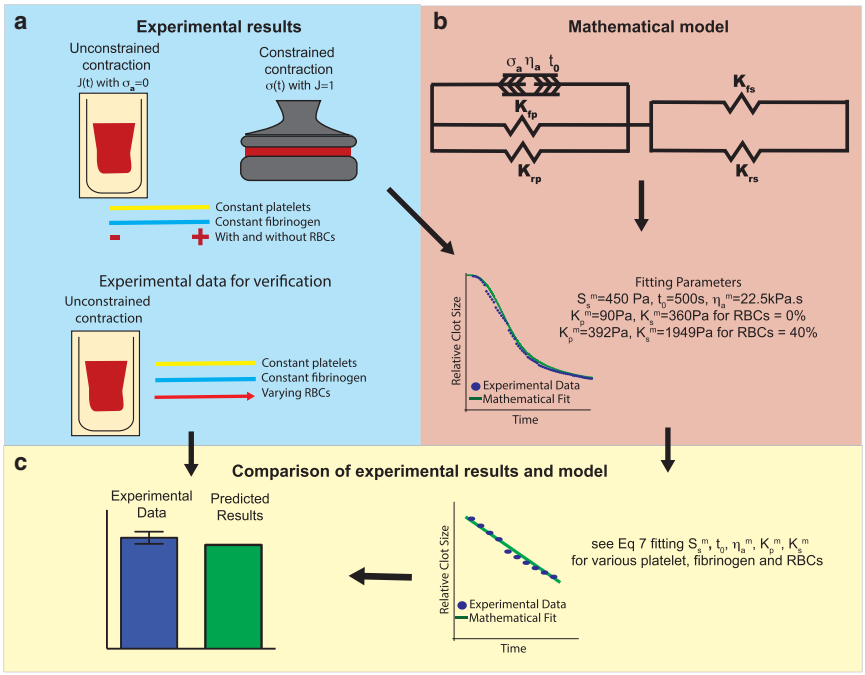

FIGURE 1 Model development and comparison with experiments. (*a* and *b*) Experimental results (*a*) and a three-element mathematical model (*b*) were combined to describe the process of clot contraction. (*c*) Independent experimental results were used to validate the predictive value of this model. σ_{stall} and η_a denote the stall stress and the active viscosity of the platelets (active element), respectively. K_{fp} and K_{rp} denote the bulk modulus of compressed fibrin and RBCs (parallel element), respectively. K_{fs} and K_{rs} denote the bulk modulus of compressed fibrin and RBCs (parallel element), respectively. All of the material properties in the three-element model were fitted using the experimental data, where *m* represents the matured blood clot and t_0 corresponds to the time of clot development. To see this figure in color, go online.

conservation of the kinetics of clot contraction across different cell types (16–18). Fibrin is a nonlinear viscoelastic material that can be modeled using a Kelvin-Voigt model (19). It is possible to theoretically understand the origin of the macroscopic viscoelastic properties of the blood clot by modeling the biopolymer as a semiflexible polymer network (20–22). The incorporation of RBCs into the blood clot volume disrupts the uniformity of the fibrin network (23), affects the mechanical properties of the clot (24), and influences the process of clot contraction (24). RBCs are easily deformed (25), and when subjected to compressive forces such as those generated by contracting platelets, they become packed in the core of the blood clot and take on a polyhedral shape (14).

Mathematical models have been used to assess the feedback effect that matrix stiffness has on the mechanics of active contractile cells (26) and to describe morphological changes and mechanical responses in an active elastic material (27). Given the structural similarities between previously described contracting microtissue and contracting blood clots, we chose to couple the basis of these aforementioned mathematical models with what is known about the individual components of clots to, for the first time to our knowledge, couple active contractile mechanics with a viscoelastic matrix (Fig. 1). The model we developed was informed by an experimental examination of contracting blood clots to further elucidate the process of clot contraction. The extent of unconstrained clot contraction for clots with varying volume fractions of RBCs was used to independently validate the predictions of the model developed here.

MATERIALS AND METHODS

The objective of this study was to develop a mathematical model that can be used to obtain information about the process of blood clot contraction. Experimental results regarding constrained and unconstrained clot contraction were used to inform the development of a model of active contractile cells interacting with a viscoelastic material (Fig. 1). Independently collected experimental results were used to validate the model.

Human blood samples

Blood samples were obtained from healthy donors after they provided informed consent in accordance with the University of Pennsylvania's institutional review board. All procedures were carried out in accordance with the approved guidelines. Platelet-rich plasma (PRP) and RBCs were obtained by centrifugation of whole citrated blood at 200 × *g* for 15 min at room temperature. Then the PRP was centrifuged at 3000 × *g* for 10 min at room temperature to obtain platelet-free plasma (PFP). RBCs were resuspended and washed three times in phosphate-buffered saline (PBS), pH 7.4. To generate samples with and without RBCs, the PRP, PFP, and RBCs were mixed to obtain constant platelet counts between parallel, donor-paired samples. Likewise, samples with varying volume fractions of RBCs were mixed to keep the platelet counts constant. Reconstituted blood samples were clotted with 1 unit/mL thrombin after addition of 2 mM $CaCl_2$ (final concentrations).

Measuring the kinetics of unconstrained clot contraction

After initiation of clot formation, samples were added to a 12 × 7 × 1 mm plastic cuvette that was prelubricated with a thin coating of 4% Triton X-100 in PBS to prevent the samples from sticking to the cuvette and allow for unconstrained clot contraction. Sample clot sizes were then tracked using a Thrombodynamics Analyzer System (HemaCore, Moscow, Russia) by accumulating digitized images based on the light-scattering properties of the clot every 15 s for 20 min (24).

Measuring contractile stress in constrained clot contraction

Clotting blood and reconstituted plasma samples were added to a rheometer with a 20-mm parallel plate (ARG2, TA Instruments, New Castle, DE). Since the samples were allowed to polymerize across a constant 400-μm gap between the plates, it was possible to measure the negative normal stress of the system continuously. This negative normal stress corresponded to the contractile force with which the constrained sample was pulling on the rheometer plate, trying to bring the two plates together.

Statistical analysis

Experimental samples were compared using a paired two-tailed Student's t-test with an α-value of 0.05 on data collected after 20 min of contraction. All statistical analysis was completed using Prism GraphPad 6.0.

RESULTS

Experimental effects of RBCs on clot contraction

We studied the time course of clot contraction by using two separate methodologies (Fig. 2). By optically tracking the light-scattering properties of the clot, we were able to follow changes in clot size during unconstrained (free to change volume) clot contraction. This experiment revealed that the addition of RBCs lessened the degree of clot contraction (Fig. 2 *c*). We conducted complementary studies using a rheometer, which allowed us to constrain the clot size (constant volume) and track the generation of contractile stress over time. In this instance, we observed that the presence of RBCs increased the contractile stress generated within the clot (Fig. 2 *f*).

Model development

Relation of the model to contracting clots

Structurally, blood clots are a collection of platelets, fibrin, and RBCs (Fig. 3 *a*), with distinct areas where fibrin and RBCs are in association with platelets, and areas where they are spatially separated from platelets (Fig. 3 *a*). To better understand how the structure and distribution of components of the clot, particularly the incorporation of RBCs, affect the process of clot contraction and the increase of contractile force, we developed a three-element model consisting of two passive viscoelastic elements and an active contractile element (Fig. 3), based on the known components of blood clots and our experimental observations (Fig. 2). The stiffness of the blood clot, which is influenced by both fibrin and RBCs, is expected to have passive components that act in parallel (Fig. 3 *c*) and in series (Fig. 3 *c*) with the active contractile element (representing the contractility of platelets). In the full model, an additional series element, accounting for platelet stiffness, platelet-platelet contact stiffness, and aligned fibrin network between platelets, is in series with the active contractile element (Fig. S7 in the Supporting Material). However, the presence of this additional element does not influence the process of clot contraction because platelets have a

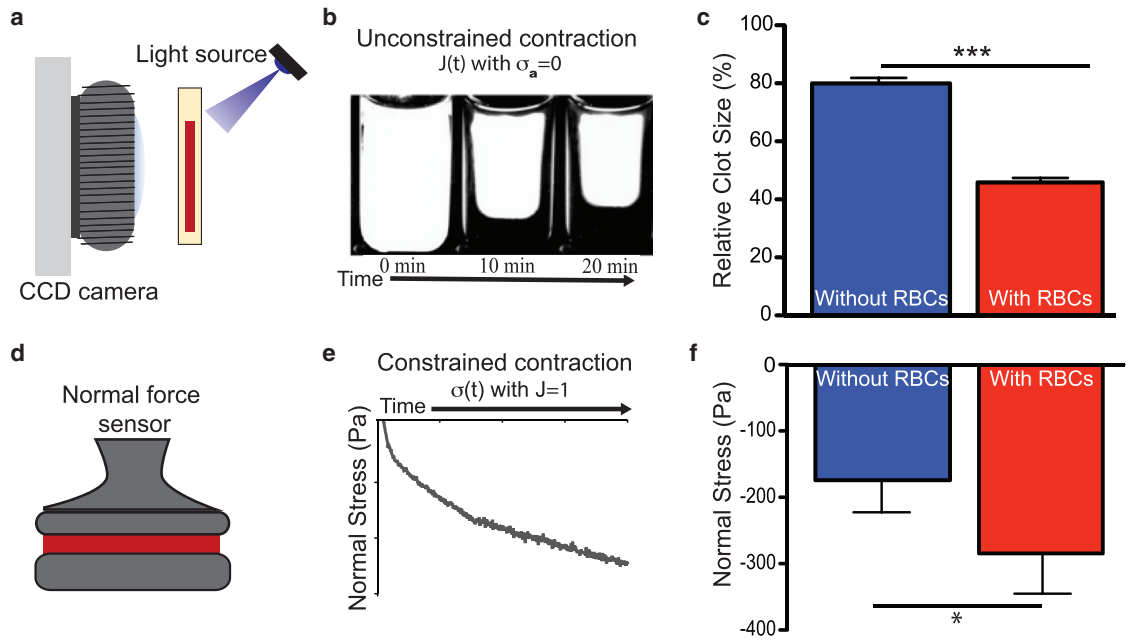

FIGURE 2 Unconstrained and constrained clot contraction. (*a–c*) Unconstrained clot contraction was tracked optically (*a*) to measure changes in clot size over time (*b*) for paired reconstituted plasma samples without RBCs and with RBCs (*c*). (*d–f*) Constrained clot contraction was assessed using a rheometer (*d*) and after the generation of negative normal stress (*e*) for paired reconstituted plasma samples without RBCs and with RBCs (*f*). Data are shown as mean ± SEM at 20 min postactivation. Statistical significance was determined using paired Student's t-tests with an α-value of 0.05. To see this figure in color, go online.

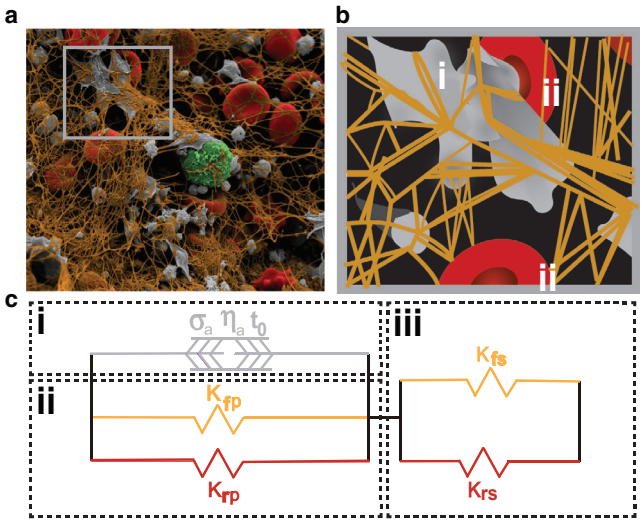

FIGURE 3 Active viscoelastic, three-element model for clot contraction. (*a* and *b*) The model was developed from scanning electron microscopy images of whole blood clots (*a*), and each component of the clot was incorporated into the model (*b*). In (*b*), platelets (*i*), fibrin (*ii*), and RBCs (*iii*) have been labeled. The three-dimensional model (represented here in one dimension) consists of three elements: an active contractile element made of platelets (*ci*), and passive parallel (*cii*) and series (*ciii*) elements made up of fibrin and RBCs. σ_a is the stress of the active elements, η_a is the viscoelastic coefficient, t_0 is the fibrin network formation time, and $K_{fp,rp,fs,rs}$ is the bulk modulus, where p represents the parallel element, s represents the series element, r corresponds to RBCs, and f corresponds to fibrin. To see this figure in color, go online.

much higher elastic modulus than fibrin (1,9,19). As such, the model can be simplified by removing this element (for details, see Supporting Materials and Methods, section G).

The initial position and the position after initiation of contraction or deformation (at time t) are given by $\boldsymbol{X}$ and $\boldsymbol{x} = \boldsymbol{x}(\boldsymbol{X}, t)$, respectively. The total deformation gradient is expressed as $\boldsymbol{F} = \partial \boldsymbol{x}/\partial \boldsymbol{X}$. The deformation gradient of the blood clot or the total strain ($\boldsymbol{F}$) is multiplicatively decomposed into the stress of the platelet-RBC-fibrin element and the RBC-fibrin element that is in series (27):

$$\boldsymbol{F} = \boldsymbol{F}_s\boldsymbol{F}_a, \quad \boldsymbol{F}_p = \boldsymbol{F}_a, \tag{1}$$

where the subscripts a, p, and s are used to denote the contributions from platelet activity, parallel passive elasticity, and series passive elasticity. Note that the parallel RBC-fibrin element deforms in parallel with the active platelet element (Fig. 3), so their deformation gradients are the same.

Properties of constitutive components

The total stress is the sum of the stress from the parallel RBC-fibrin and contractile platelet components (27):

$$\boldsymbol{\sigma} = \boldsymbol{\sigma}_a(\boldsymbol{F}_a) + \boldsymbol{\sigma}_p(\boldsymbol{F}_p) = \boldsymbol{\sigma}_s(\boldsymbol{F}_s). \tag{2}$$

Note that the stress in the series RBC-fibrin element is the same as the total stress (Fig. 3). The constitutive laws for each mechanical component are considered to relate the stress at any material point to deformation.

We use the neo-Hookean hyperelastic stress-strain relations to model the passive strain-hardening response of the series and parallel elements:

$$\boldsymbol{\sigma}_p = K_p\frac{\ln J_p}{J_p}\boldsymbol{I} + G_p\,\mathrm{dev}\left(\frac{\boldsymbol{B}_p}{J_p^{2/3}}\right), \tag{3}$$

$$\boldsymbol{\sigma}_s = K_s\frac{\ln J_s}{J_s}\boldsymbol{I} + G_s\,\mathrm{dev}\left(\frac{\boldsymbol{B}_s}{J_s^{2/3}}\right),$$

where $J = \det(\boldsymbol{F})$, $\boldsymbol{B} = \boldsymbol{F}\boldsymbol{F}^T$ are the Jacobians representing the relative volume change and the left Cauchy Green deformation tensor, respectively, and K and G are the initial bulk and shear moduli, respectively.

Recent experiments showed that contractile cells (e.g., fibroblasts) subjected to uniaxial loading have an active stress versus strain-rate response that obeys the classic Hill relation (18,28). As in other contractile cells, contraction in platelets involves myosin-actin interactions (29). According to the Hill relation, the rate of contraction is largest in the absence of any applied stress, monotonically decreases with increasing applied stress, and eventually vanishes when the applied stress reaches the stall stress (28). Therefore, in our three-dimensional, large-deformation analysis, we assume that the rate of active deformation, $\boldsymbol{D}_a$ depends on the active stress, $\boldsymbol{\sigma}_a$ (18):

$$\boldsymbol{D}_a = \frac{1}{2}\left(\dot{\boldsymbol{F}}_a\boldsymbol{F}_a^{-1} + \left(\dot{\boldsymbol{F}}_a\boldsymbol{F}_a^{-1}\right)^T\right) = \frac{1}{\eta_a}\left(\boldsymbol{\sigma}_a - \frac{\sigma_{stall}}{J_a^{2/3}}\boldsymbol{I}\right), \tag{4}$$

where $J = \det(\boldsymbol{F})$ is the Jacobian representing the relative volume change, η_a is the active viscosity, and σ_{stall} is the stall stress, which we assume to be isotropic. The active viscosity of the blood clot has the same mathematical form as that of a viscoelastic material, but arises from the Hill relation (which postulates that the contraction rate linearly decreases with stress) of platelet contraction rather than the viscoelasticity of fibrin networks.

Although fibrin and RBCs are viscoelastic in nature, they are modeled as elastic materials due to the elastic nature of their mechanical response at low levels of strain rate (Supporting Materials and Methods, section H). As fibrin has been shown to behave as a semiflexible polymer (20,21), it is possible to determine the theoretical bulk and shear moduli for fibrin alone (Supporting Materials and Methods, section B), which are in agreement with reported experimental mechanical properties of fibrin (11,30). This can be used transitively to determine the development of the fibrin network (19). As the propagation of the platelet-generated contractile force through the volume of the clot

is highly dependent on the presence of fibrin, it is reasonable to assume that the timescale onset is similar for both fibrin network formation and clot contraction (Supporting Materials and Methods, section B).

Active and poroelastic limits

As clot contraction results in the expulsion of serum from the volume of the blood clot, it was critical to determine whether the dynamics of clot contraction is due to the activation limit associated with active contraction of a viscoelastic material or to the diffusion limit associated with a poroelastic material. Therefore, we developed an active-poroelastic model to consider the expulsion of serum from the blood clot (Supporting Materials and Methods, section A; Fig. S1). The extent of unconstrained contraction was found to be independent of size, as no significant differences occurred over a range of volumes (Fig. 4), which showed that the clot for the characteristic size used in this study was active viscoelastic rather than poroelastic. This can be captured with the three-element model we used here (Supporting Materials and Methods, section D; Fig. 4). As the sample size is comparable to the intrinsic material length scale, $(k\eta_a/\eta_{sol})^{1/2}$, the viscoelasticity and poroelasticity must be considered simultaneously. The clot contraction dynamics is governed by the viscoelasticity of the clot for smaller volumes, whereas larger clot volumes are better described by the poroelastic limit. The visco-poroelastic model can also describe polymeric gels by accounting for both solvent migration and viscoelastic deformation (31). Macroscopic biological (32) and semi-interpenetrating network (33) gels have a relatively long viscoelastic relaxation time compared with that needed for solvent migration through a relatively long distance, which can be predicted by a poroelastic model.

Contraction dynamics

The constitutive equations (Eqs. 1–4), the equilibrium condition $(\partial\boldsymbol{\sigma_{ij}}/\partial\boldsymbol{x_j} = 0)$, the initial stress-free condition, and the unconstrained or constrained boundary conditions constitute a well-posed initial value problem (Supporting Materials and Methods, section A). The boundary conditions used here allow the shear modulus to be removed from Eq. 3, as shear deformation does not play a role in blood clots that are not under fluid flow. Since the time progression of the stress and deformation gradients is homogeneous and isotropic, the constitutive equations can be simplified as (Supporting Materials and Methods, section E)

$$\sigma = \sigma_a + \sigma_p = \sigma_s, \quad J = J_s J_a, \tag{5}$$

$$\sigma_a = \left(\frac{\sigma_{stall}}{J_a^{2/3}} + \frac{\eta_a}{3J_a}\frac{dJ_a}{dt}\right), \quad \sigma_p = K_p\frac{\ln(J_a)}{J_a}, \quad \sigma_s = K_s\frac{\ln(J_s)}{J_s}.$$

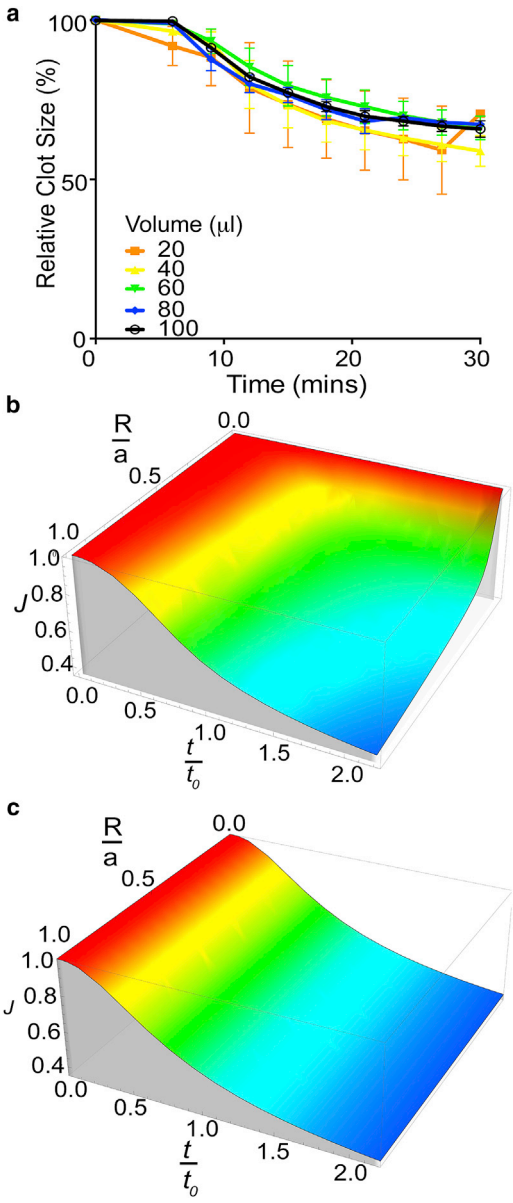

FIGURE 4 Clots undergoing unconstrained contraction behave as an active viscoelastic material, not a poroelastic material. (*a*) Unconstrained clot contraction for volumes ranging from 10 to 100 μL revealed no difference in relative clot size at the measured time points. Statistical significance was assessed using a repeated-measures analysis of variance. (*b* and *c*) A computational comparison of the (*b*) activation time and (*c*) poroelastic diffusion time revealed that clot contraction is not a result of poroelastic diffusion due to the length scale of the diffusion. The relative volume ratio of the blood clot, J, is a function of the scaled radius, a/R, and scaled time, t/t_0, using the spherically symmetric model for the activation limit (*b*) and the poroelastic limit (*c*). Here R and a denote the radial distance from the center and the initial radius of the clot, respectively. To see this figure in color, go online.

The active contractile stress (σ_a) generated by the platelets is balanced with the tension of the series element (σ_s) and the compression of the parallel element (σ_p). The total stress (σ) is the same as the tension of the series element (σ_s)

(Fig. 3). Note that the mechanical properties of contracting blood clots are dependent on time (Supporting Materials and Methods, section E):

$$\frac{K_p}{K_p^m} = \frac{K_s}{K_s^m} = \frac{\eta_a}{\eta_a^m} = \frac{\sigma_{stall}}{S_s^m\left(1-e^{-\frac{t}{t_0}}\right)^2} = \left(1-e^{-\frac{t}{t_0}}\right)^2, \quad (6)$$

where K_p^m and K_s^m are the bulk moduli of the parallel and series elements, respectively; S_s^m and η_a^m are the stall stress and viscosity of platelets for clot, respectively; and t_0 corresponds to the time of clot development. The stiffness of the fibrin network is time dependent during network formation or maturation. The superscript m denotes the variables for the matured fibrin network.

Unconstrained clot contraction

In unconstrained blood clot contraction, as studied through optical tracking, the net applied stress at all times points is equal to zero and does not depend on the series element (Eq. 2). As such, the boundary condition for this homogeneous and isotropic deformation is $\sigma(t) = 0$. This allows for elucidation of the parameters affecting the parallel element:

$$J^{1/3}\left(1-e^{-\frac{t}{t_0}}\right)^2 + \frac{1}{3}\frac{\eta_a^m}{S_s^m}\frac{dJ_a}{dt} + \frac{K_p^m}{S_s^m}\ln(J) = 0 \quad (7)$$

where K_p^m/S_s^m, η_a^m/S_s^m, and t_0 can be determined by fitting the computed degree of contraction $(J^{2/3})$ over time to the experimental results (Supporting Materials and Methods, section E). For $t \gg t_0$, the scaled equilibrium Jacobian can be derived from Eq. 7:

$$\frac{K_p^m}{S_s^m}\ln(J) + J^{1/3} = 0. \quad (8)$$

We find that the relative clot size, $J^{2/3}$, increases with increasing scaled parallel stiffness, K_p^m/S_s^m.

Constrained clot contraction

To assess constrained contraction using a rheometer, the clot volume is kept constant and the contractile stress is allowed to change over time. Since the parameters describing the parallel element are determined through the fitting of unconstrained clot contraction, constrained contraction can be used to determine the parameters that affect the series element:

$$\frac{\sigma}{S_s^m}\frac{1}{\left(1-e^{-\frac{t}{t_0}}\right)^2} = \left[\frac{1}{J_a^{2/3}}\left(1-e^{-\frac{t}{t_0}}\right)^2 + \frac{1}{3J_a}\frac{\eta_a^m}{S_s^m}\frac{dJ_a}{dt} + \frac{K_p^m}{S_s^m}\frac{\ln(J_a)}{J_a}\right] = -\frac{K_s^m}{S_s^m}\ln(J_a)J_a, \quad (9)$$

where S_s^m and K_s^m/S_s^m can be determined by fitting the computed total stress (σ) versus time (t) curves to actual experimental results (Supporting Materials and Methods, section E).

For $t \gg t_0$, the scaled equilibrium stress can be derived from Eq. 9:

$$\frac{\sigma}{S_s^m} = \left[\frac{1}{J_a^{2/3}} + \frac{K_p^m}{S_s^m}\frac{\ln(J_a)}{J_a}\right] = -\frac{K_s^m}{S_s^m}\ln(J_a)J_a. \quad (10)$$

We find that the scaled equilibrium stress, σ/S_s^m, decreases with increasing scaled parallel stiffness, K_p^m/S_s^m, and increases with increasing scaled series stiffness, K_s^m/S_s^m.

Linear analysis

The key features of the unconstrained and constrained clot contraction observed in our experiments can be understood quantitatively through the use of linear analysis on equilibrium clots $(t \gg t_0)$. The volumetric strain, $\varepsilon_v = J - 1 \ll 1$, for small deformation; the equilibrium volumetric strain, $\overline{\varepsilon}_v$, for unconstrained contraction; and the equilibrium total stress, $\overline{\sigma}$, for constrained contraction can be simplified from Eqs. 6 and 7, respectively:

$$\overline{\varepsilon}_v = -\frac{S_s^m}{K_p^m}, \quad \frac{\overline{\sigma}}{S_s^m} = \frac{1}{1+\frac{K_p^m}{K_s^m}}. \quad (11)$$

The equilibrium volumetric strain, ε_v, increases with parallel stiffness, K_p^m, which is consistent with the experimental result that the addition of RBCs lessened the degree of clot contraction (Figs. 2 and 5). The equilibrium total stress, $\overline{\sigma}$, increases with decreasing parallel stiffness, K_p^m, or increasing series stiffness, K_s^m. As the increase of series stiffness is more significant than that of parallel stiffness, the presence of RBCs increases the generation of contractile stress within the clot. The equilibrium degree of contraction and total stress for finite deformation can be numerically solved from Eqs. 7 and 9 as $t \gg t_0$, which shows the same trend as the linear analysis.

Comparison with time-course experimental data

To assess the validity of our model, we compared the experimental curves with curves obtained through linear analysis (Supporting Materials and Methods, section F). Similar

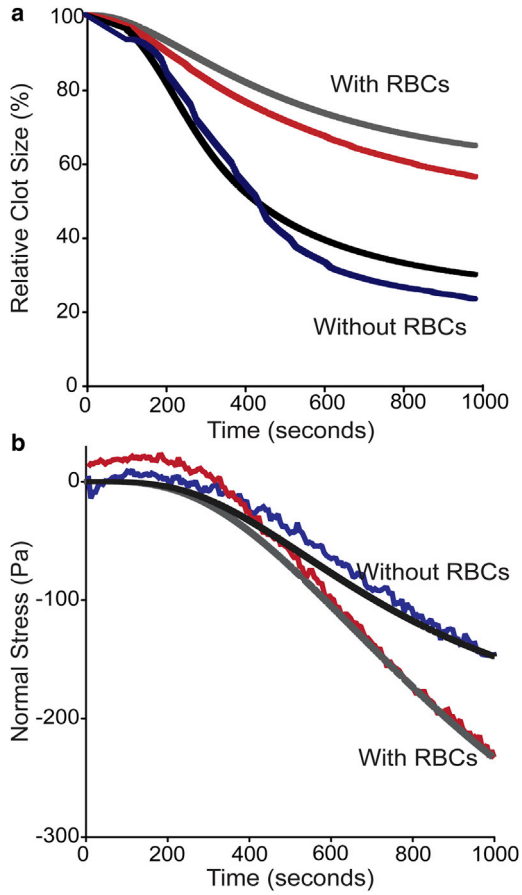

FIGURE 5 Comparison of experimental and modeled clot contraction. (*a*) Unconstrained clot contraction was tracked for 20 min by recording the change in clot size. Contraction was followed for reconstituted samples with platelets and fibrin alone (labeled without RBCs) and with the addition of RBCs (labeled with RBCs). Likewise, unconstrained contraction was calculated using the three-element model, taking into account the presence and absence of RBCs. (*b*) Constrained clot contraction was tracked for 20 min by recording the generation of contractile force (negative) using a high-precision rheometer. Contraction was followed for reconstituted samples with platelets and fibrin alone (labeled without RBCs) and with the addition of RBCs (labeled with RBCs). Constrained contraction was calculated using the three-element model, taking into account the presence and absence of RBCs. To see this figure in color, go online.

concentrations and mechanical properties of the clot components were used in the experiments and the model (Table S1). By tracking the changes in clot size over time, we were able to quantify the dynamics of unconstrained clot contraction, and found that the presence of RBCs resulted in a reduced extent of clot contraction. A comparison of the experimental data and the data generated by our three-element model reveals that they are in close agreement (Fig. 5).

The contractile stress generated by the platelets is measured using a precise rheometer. When the clot polymerizes, it is adherent to the upper and lower plates of the rheometer, thus allowing measurement of the negative normal stress during constrained contraction. As the clot volume is constant, it is possible to track the force with which the platelets are contracting. In the presence of RBCs, the platelet-fibrin meshwork generates larger contractile forces compared with platelets and fibrin alone. A comparison of the experimental data and those obtained through our model reveals contraction following similar trends (Fig. 5). Extension of the duration of constrained contraction revealed that samples in the absence of RBCs reached a stall stress at ~25 min, whereas those in the presence of RBCs reached a stall stress at ~40 min (Fig. S5).

Model verification

To verify the model we developed, we collected independent experimental data with a range of volume fractions of RBCs (<10%, 15–20%, 30–40%, and >40%). Experimental results showed that the extent of clot contraction varied inversely with the volume fraction of RBCs (Fig. 6). We compared the experimental extent of clot contraction with the extent of clot contraction that was predicted by the model using 200,000 μL^{-1} platelets, 2.5 mg/mL fibrinogen, and varying volume fractions of RBCs (Fig. 6). The predicted values are within the SD of the experimental data for the tested ranges of volume fraction of RBCs, showing that the model is in close agreement with experimental results and can be used to predict how changes in clot composition affect clot contraction.

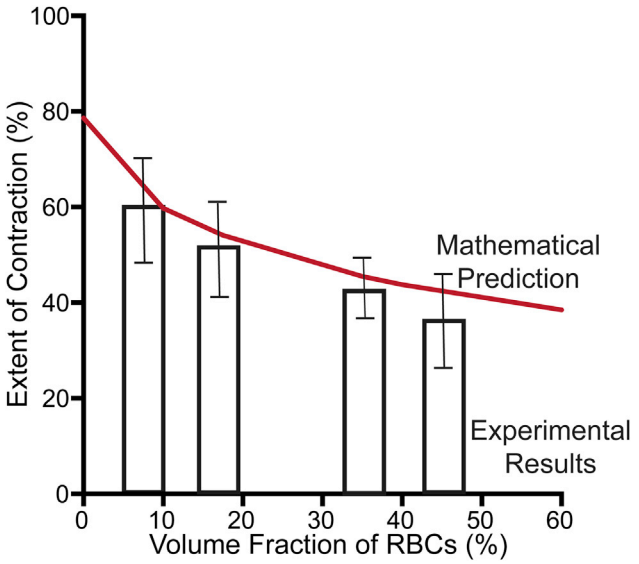

FIGURE 6 Validation of the clot contraction model. Unconstrained clot contraction was tracked optically for 20 min at varying volume fractions of RBCs (<10%, 15–20%, 30–40%, and >40%, represented as bars). Data are shown as mean ± SD. The model was used to predict the extent of clot contraction at 20 min for 200,000 μL^{-1} platelets, 2.5 mg/mL fibrinogen, and varying volume fractions of RBCs. The predicted extent of clot contraction for volume fractions ranging from 0% RBCs to 60% RBCs is represented by the solid line. To see this figure in color, go online.

DISCUSSION

Our study of clot contraction reveals that the presence of RBCs in the clot volume results in an increase in the magnitude of contractile force generated by the platelet-fibrin meshwork and a reduction in the overall extent of contraction. Clot contraction has been shown to be important for the restoration of blood flow past otherwise obstructive thrombi (15). It is known that mortality after a thrombotic event can be correlated with the composition of the thrombus and the presence of RBCs in the clot volume (34). The ability to examine how the presence of RBCs affects the compaction of a thrombus, and consequently the blood flow past the thrombus, has the potential to guide future therapeutic applications for patients with pathological conditions associated with increased (polycythemia) or reduced (anemia and hemodilution) RBC counts in the blood.

By studying a combination of unconstrained and constrained clot contraction, we developed a macroscopic three-element model that couples active contractile cells with a passive viscoelastic matrix. Due to the conservation of contractile machinery between varying cell types, this novel, to our knowledge, model has implications far beyond blood clot contraction and can inform a variety of fields in which active contractile cells are resisted by and interacting with a viscoelastic matrix. For example, during wound healing, contractile myofibroblasts interact with a fibrous extracellular matrix, but it is known that endothelial, epithelial, and inflammatory cells are present in the wound bed (35,36). As our model revealed that the presence of cells in the viscoelastic matrix influences the active contraction of cells, the proportion and type of cells that are present in the wound bed may affect the contraction of myofibroblasts.

Contractile cells such as fibroblasts, myoblasts, and platelets have been shown to individually generate contractile forces ranging from 0.1 to 300 nN/cell (1,18,37,38). The accumulation of force generated by these individual active contractile cells results in a macroscopic contraction of the matrix. Although it is known that cells can sense and respond differently based on the stiffness of the surrounding matrix (1,2), our results reveal that the composition and distribution of the matrix can influence the force and extent of macroscopic contraction.

Lam et al. (1) previously showed in single-cell studies that platelets are able to generate forces ranging from 1.5 to 79 nN per cell, with the average cell generating forces of 20 nN. Data generated by our experiments and the three-element model indicate that platelets are able to generate contractile stresses of 175 and 300 Pa in the absence and presence of RBCs, respectively. Based on an average platelet count of 200,000 μL^{-1}, we found that individual cells were generating forces of ~51 nN/platelet in the absence of RBCs and ~88 nN/platelet in the presence of RBCs. Likewise, Lam et al. (1) observed that platelets generated greater contractile force varies with increased substrate stiffness. Since RBCs are known to alter fibrin structure and hence matrix stiffness (23), it is not surprising that the addition of RBCs has the potential to influence the extent and force of clot contraction.

Our combination of an active contractile component and a passive viscoelastic material reveals that the active component is affected not only by the stiffness of the viscoelastic matrix, as modulated through the addition of RBCs, but also by the distribution of the RBCs within the passive elements (Eq. 4). The influence of RBCs on the parallel stiffness results in a compressive resistance and transitively a reduced degree of contraction (Fig. 7 *d*), whereas the influence on the series stiffness results in a tensile resistance to contraction, which influences the stall stress and results in an increased contractile force generated by the platelet-fibrin network (Fig. 7 *e*).

The validation of the three-element model developed with varying volume fractions of RBCs (Fig. 6) shows that our model can be used to predict how changes in the composition and spatial nonuniformity of a blood clot influence the process of clot contraction. By combining experimental results with the model we developed, we were able to distinguish between and develop equations for both constrained and unconstrained clot contraction.

This validated model lays the groundwork needed for an examination of in vivo blood clot contraction where portions of the clot are constrained through attachment to the vessel wall and other portions are unconstrained, and provides vital information about differences in clot contraction based on the structure of in vivo blood clots. Although others have modeled fluid flow over blood clots (39), they have not accounted for active contraction of the blood clots. By modifying the boundary conditions of our model, we will be able to examine contracting blood clots under shear forces such as those that would occur in vivo.

Collectively, our results reveal that clot contraction dynamics is dominated by the active contraction of platelets interacting with a viscoelastic material, and not by the poroelastic nature of fibrin. The addition of RBCs to the matrix results in an increase in the series and parallel stiffness, as well as changes in the tensile and compressive resistance and the applied contractile force, showing that the presence of RBCs can influence the process of clot contraction. By analyzing the time evolution of volumetric contraction and contractile stress of unconstrained and constrained clots, we developed a validated model of active contractile cells interacting with a passive viscoelastic material. In the future, we hope to integrate this model with methods to calculate fluid shear stresses acting on the surface of the clot to analyze the stability of blood clots in the presence of flow.

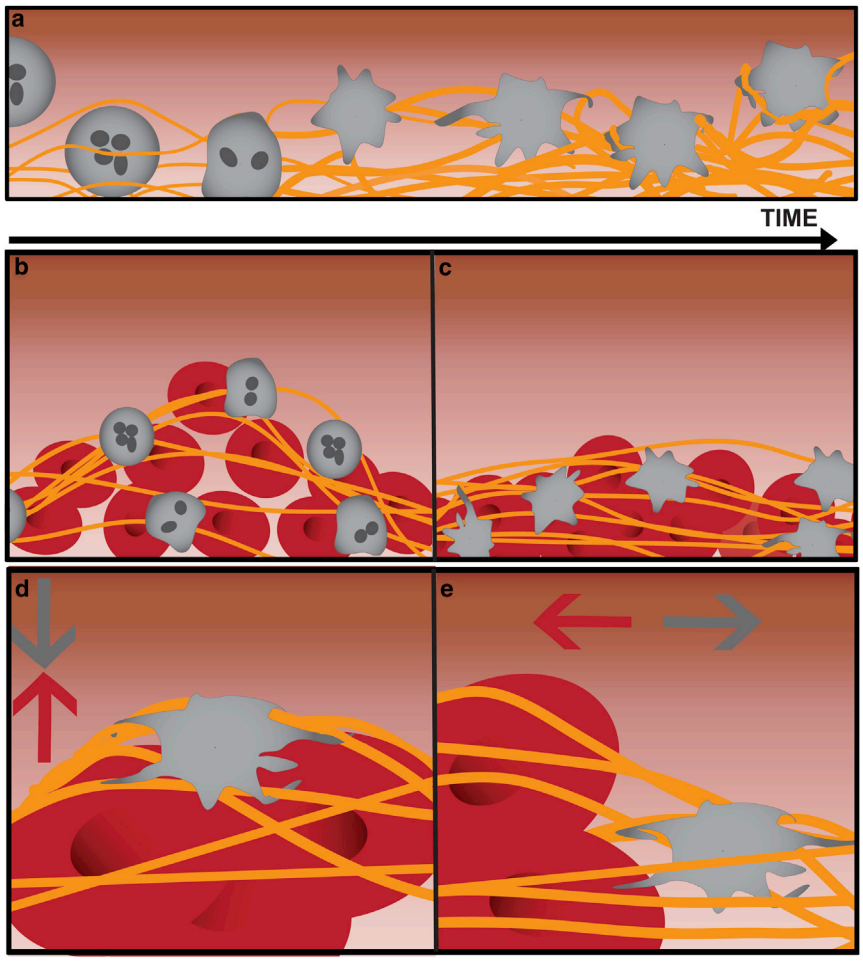

FIGURE 7 Effect of RBCs on clot contraction. (*a*) As time progresses, platelet activation and the development of the fibrin network occur simultaneously. (*b–d*) The contractile force generated and propagated through the platelet-fibrin meshwork is affected by the presence of RBCs (*b*), which will ultimately become compacted due to the contractile force, resulting in the volumetric shrinkage of the clot (*c*). Linear static analysis reveals that larger parallel stiffness, which is due to more blood cells, results in compressive resistance and a reduced degree of clot contraction (*d*). (*e*) A larger series stiffness, induced by the presence of more cells, results in a tensile resistance, disruption of the stall stress, and consequently a larger normal force. Too see this figure in color, go online.

SUPPORTING MATERIAL

Supporting Materials and Methods, nine figures, and one table are available at http://www.biophysj.org/biophysj/supplemental/S0006-3495(17)30044-9.

AUTHOR CONTRIBUTIONS

V.B.S. and J.W.W. designed experiments. V.T. and R.I.L. performed experiments. H.W., V.T., and V.B.S. analyzed data and developed the mathematical model. V.T., H.W., J.W.W., and V.B.S. wrote the manuscript.

ACKNOWLEDGMENTS

This work was supported by National Institutes of Health grants R01EB017753, U01CA202177, U54CA193417, UO1HL116330, HL090774, and T32 H10791; National Science Foundation grants DMR1505662 and CMMI-1548571; American Heart Association grant 16PRE30260002 (V.T.); and the Thousand Young Talents Program of China.

REFERENCES

1. Lam, W. A., O. Chaudhuri, …, D. A. Fletcher. 2011. Mechanics and contraction dynamics of single platelets and implications for clot stiffening. *Nat. Mater.* 10:61–66.
2. Qiu, Y., A. C. Brown, …, W. A. Lam. 2014. Platelet mechanosensing of substrate stiffness during clot formation mediates adhesion, spreading, and activation. *Proc. Natl. Acad. Sci. USA.* 111:14430–14435.
3. Carr, M. E., Jr., E. J. Martin, and S. L. Carr. 2002. Delayed, reduced or inhibited thrombin production reduces platelet contractile force and results in weaker clot formation. *Blood Coagul. Fibrinolysis.* 13:193–197.
4. Jennings, L. K., J. E. Fox, …, D. R. Phillips. 1981. Changes in the cytoskeletal structure of human platelets following thrombin activation. *J. Biol. Chem.* 256:6927–6932.
5. Nakata, T., and N. Hirokawa. 1987. Cytoskeletal reorganization of human platelets after stimulation revealed by the quick-freeze deep-etch technique. *J. Cell Biol.* 105:1771–1780.
6. Weisel, J. W. 2005. Fibrinogen and fibrin. *Adv. Protein Chem.* 70:247–299.
7. Weisel, J. W., and R. I. Litvinov. 2013. Mechanisms of fibrin polymerization and clinical implications. *Blood.* 121:1712–1719.
8. Brown, A. E. X., R. I. Litvinov, …, J. W. Weisel. 2009. Multiscale mechanics of fibrin polymer: gel stretching with protein unfolding and loss of water. *Science.* 325:741–744.
9. Kim, O. V., R. I. Litvinov, …, M. S. Alber. 2014. Structural basis for the nonlinear mechanics of fibrin networks under compression. *Biomaterials.* 35:6739–6749.
10. Ehrlicher, A., and J. H. Hartwig. 2011. Cell mechanics: contracting to stiffness. *Nat. Mater.* 10:12–13.

11. Wufsus, A. R., K. Rana, …, K. B. Neeves. 2015. Elastic behavior and platelet retraction in low- and high-density fibrin gels. *Biophys. J.* 108:173–183.
12. Stalker, T. J., J. D. Welsh, …, L. F. Brass. 2014. A systems approach to hemostasis: 3. Thrombus consolidation regulates intrathrombus solute transport and local thrombin activity. *Blood.* 124:1824–1831.
13. Carr, M. E., Jr. 2003. Development of platelet contractile force as a research and clinical measure of platelet function. *Cell Biochem. Biophys.* 38:55–78.
14. Cines, D. B., T. Lebedeva, …, J. W. Weisel. 2014. Clot contraction: compression of erythrocytes into tightly packed polyhedra and redistribution of platelets and fibrin. *Blood.* 123:1596–1603.
15. Muthard, R. W., and S. L. Diamond. 2012. Blood clots are rapidly assembled hemodynamic sensors: flow arrest triggers intraluminal thrombus contraction. *Arterioscler. Thromb. Vasc. Biol.* 32:2938–2945.
16. Huxley, A. F. 1957. Muscle structure and theories of contraction. *Prog. Biophys. Biophys. Chem.* 7:255–318.
17. Debold, E. P., J. B. Patlak, and D. M. Warshaw. 2005. Slip sliding away: load-dependence of velocity generated by skeletal muscle myosin molecules in the laser trap. *Biophys. J.* 89:L34–L36.
18. Mitrossilis, D., J. Fouchard, …, A. Asnacios. 2009. Single-cell response to stiffness exhibits muscle-like behavior. *Proc. Natl. Acad. Sci. USA.* 106:18243–18248.
19. van Kempen, T. H. S., A. C. B. Bogaerds, …, F. N. van de Vosse. 2014. A constitutive model for a maturing fibrin network. *Biophys. J.* 107:504–513.
20. MacKintosh, F. C., J. Käs, and P. A. Janmey. 1995. Elasticity of semiflexible biopolymer networks. *Phys. Rev. Lett.* 75:4425–4428.
21. Gittes, F., and F. C. MacKintosh. 1998. Dynamic shear modulus of a semiflexible polymer network. *Phys. Rev. E Stat. Phys. Plasmas Fluids Relat. Interdiscip. Topics.* 58:R1241.
22. Janmey, P. A., M. E. McCormick, …, F. C. MacKintosh. 2007. Negative normal stress in semiflexible biopolymer gels. *Nat. Mater.* 6:48–51.
23. Gersh, K. C., C. Nagaswami, and J. W. Weisel. 2009. Fibrin network structure and clot mechanical properties are altered by incorporation of erythrocytes. *Thromb. Haemost.* 102:1169–1175.
24. Tutwiler, V., R. I. Litvinov, …, J. W. Weisel. 2016. Kinetics and mechanics of clot contraction are governed by the molecular and cellular composition of the blood. *Blood.* 127:149–159.
25. Khairy, K., J. Foo, and J. Howard. 2010. Shapes of red blood cells: comparison of 3D confocal images with the bilayer-couple model. *Cell. Mol. Bioeng.* 1:173–181.
26. Shenoy, V. B., H. Wang, and X. Wang. 2016. A chemo-mechanical free-energy-based approach to model durotaxis and extracellular stiffness-dependent contraction and polarization of cells. *Interface Focus.* 6:20150067.
27. Wang, H., A. A. Svoronos, …, V. B. Shenoy. 2013. Necking and failure of constrained 3D microtissues induced by cellular tension. *Proc. Natl. Acad. Sci. USA.* 110:20923–20928.
28. Hill, A. V. 1938. The heat of shortening and the dynamic constants of muscle. *Proc. Natl. Acad. Sci. USA.* 126:136–195.
29. Cohen, I. 1979. The contractile system of blood platelets and its function. *Methods Achiev. Exp. Pathol.* 9:40–86.
30. Litvinov, R. I., and J. W. Weisel. 2016. Fibrin mechanical properties and their structural origins. *Matrix Biol.*, S0945-053X(16)30184-6.
31. Wang, X., and W. Hong. 2012. A visco-poroelastic theory for polymeric gels. *Proc. R Soc. A Math. Phy. Eng. Sci.* 468:3824–3841.
32. Roberts, J. J., A. Earnshaw, …, S. J. Bryant. 2011. Comparative study of the viscoelastic mechanical behavior of agarose and poly(-ethylene glycol) hydrogels. *J. Biomed. Mater. Res. B Appl. Biomater.* 99:158–169.
33. Liu, Y., and M. B. Chan-Park. 2009. Hydrogel based on interpenetrating polymer networks of dextran and gelatin for vascular tissue engineering. *Biomaterials.* 30:196–207.
34. Quadros, A. S., E. Cambruzzi, …, R. D. Lopes. 2012. Red versus white thrombi in patients with ST-elevation myocardial infarction undergoing primary percutaneous coronary intervention: clinical and angiographic outcomes. *Am. Heart J.* 164:553–560.
35. Rodero, M. P., and K. Khosrotehrani. 2010. Skin wound healing modulation by macrophages. *Int. J. Clin. Exp. Pathol.* 3:643–653.
36. Diegelmann, R. F., and M. C. Evans. 2004. Wound healing: an overview of acute, fibrotic and delayed healing. *Front. Biosci.* 9:283–289.
37. Freyman, T. M., I. V. Yannas, …, L. J. Gibson. 2001. Micromechanics of fibroblast contraction of a collagen-GAG matrix. *Exp. Cell Res.* 269:140–153.
38. Delvoye, P., P. Wiliquet, …, C. M. Lapière. 1991. Measurement of mechanical forces generated by skin fibroblasts embedded in a three-dimensional collagen gel. *J. Invest. Dermatol.* 97:898–902.
39. Fogelson, A. L., and K. B. Neeves. 2015. Fluid mechanics of blood clot formation. *Annu. Rev. Fluid Mech.* 47:377–403.

Biophysical Journal, Volume *112*

Supplemental Information

Interplay of Platelet Contractility and Elasticity of Fibrin/Erythrocytes in Blood Clot Retraction

Valerie Tutwiler, Hailong Wang, Rustem I. Litvinov, John W. Weisel, and Vivek B. Shenoy

Supplementary Materials

A. 3D active-poroelastic Model

To quantitatively analyze the dynamics of contracting blood clots, we designed an active-poroelastic model that consists of two passive elastic elements to represent the elasticity of the fibrin network and the RBCs, an active contractile element, and a porous element, as shown in Supplemental Fig. 1. The stiffness of the blood clot, including the fibrin network and erythrocytes, is expected to have components that act in series and in parallel to the active contractile element (representing the contractility of platelets). The porous element, which accounts for the contribution due to expulsion of the plasma, is added in parallel with the other elements. With position vectors to a material point in the reference and current configurations (at time t) given by $\boldsymbol{X}$ and $\boldsymbol{x} = \boldsymbol{x}(\boldsymbol{X}, t)$, respectively, the total deformation gradient tensor is expressed as $\boldsymbol{F} = \partial \boldsymbol{x}/\partial \boldsymbol{X}$. A reference state is assigned when the clot is stress-free and the solvent (plasma) in the clot is in equilibrium with the pure liquid solvent. In the reference state, the clot is undeformed ($\boldsymbol{F} = 1$), the chemical potential of plasma in the gel is set to be zero ($\mu = 0$), and the concentration of plasma is denoted by C_0. The deformation gradient of the blood clot ($\boldsymbol{F}$) is multiplicatively decomposed into active contractile ($\boldsymbol{F_a}$) and series passive components ($\boldsymbol{F_s}$),*(1)*

$$\boldsymbol{F} = \boldsymbol{F_s F_a},\ \boldsymbol{F_p} = \boldsymbol{F_a},\ \boldsymbol{F_{sol}} = \boldsymbol{F}, \tag{1}$$

where the subscripts *a*, *p*, *s*, and *sol* are used to denote the contributions from platelet activity, parallel passive elasticity, series passive elasticity, and the contribution from plasma, respectively. Note that the parallel element deforms in parallel with the active

element, and the porous element deforms in parallel with the other elements, so their deformation gradients are the same.

The total stress at a material point is the sum of the stress from the parallel passive, contractile, and porous components,

$$\boldsymbol{\sigma} = \boldsymbol{\sigma_a} + \boldsymbol{\sigma_p} + \boldsymbol{\sigma_{sol}},$$

$$\boldsymbol{\sigma_s} = \boldsymbol{\sigma_a} + \boldsymbol{\sigma_p}. \qquad (2)$$

Note that the stress in the series passive element is the sum of the contractile stress and the parallel passive element. The constitutive laws for each mechanical component are considered to relate the stress at any material point to deformation.

We use the neo-Hookean hyperelastic stress-strain relations to describe the passive strain-hardening response of the parallel and series elements,

$$\boldsymbol{\sigma_p} = K_p \frac{\ln J_p}{J_p} \boldsymbol{I} + G_p \,\mathrm{dev}\left(\frac{\boldsymbol{B_p}}{{J_p}^{2/3}}\right), \qquad (3)$$

$$\boldsymbol{\sigma_s} = K_s \frac{\ln J_s}{J_s} \boldsymbol{I} + G_s \,\mathrm{dev}\left(\frac{\boldsymbol{B_s}}{{J_s}^{2/3}}\right),$$

where $J = \det(\boldsymbol{F})$, $\boldsymbol{B} = \boldsymbol{F}\boldsymbol{F}^{\boldsymbol{T}}$ are the Jacobian representing the relative volume change and the left Cauchy Green deformation tensor, respectively, and K and G are the initial bulk and shear moduli, respectively.

Recent experiments on fibroblasts*(2)* subject to uniaxial loading have shown that their active stress vs. strain-rate response obeys the classic Hill relation*(3)*. Therefore, in our 3D large-deformation analysis, we assume that the rate of active deformation, $\boldsymbol{D_a}$ depends on the active stress, $\boldsymbol{\sigma_a}$,

$$\boldsymbol{D_a} = \frac{1}{2}\left(\dot{\boldsymbol{F}}_{\boldsymbol{a}}\boldsymbol{F}_{\boldsymbol{a}}^{-\mathbf{1}} + (\dot{\boldsymbol{F}}_{\boldsymbol{a}}\boldsymbol{F}_{\boldsymbol{a}}^{-\mathbf{1}})^{T}\right) = \frac{1}{\eta_a}\left(\boldsymbol{\sigma_a} - \frac{\sigma_s}{{J_a}^{2/3}}\boldsymbol{I}\right), \quad (4)$$

where η_a is the active viscosity, and σ_s is the stall stress, which we assume to be isotropic.

Since biological materials satisfy the criterion of molecular incompressibility *(4)* (i.e. any change in the volume of the clot is due to the flow of plasma), the stress and relative change in plasma volume can be expressed as

$$\boldsymbol{\sigma_{sol}} = -\frac{\mu}{\Omega}\boldsymbol{I}, \quad (5)$$

$$J_{sol} = 1 + (C - C_0)\Omega,$$

where μ is chemical potential of the plasma, and Ω is its molar volume. $\boldsymbol{I}$ is identify tensor and C and C_0 are the current and reference plasma concentrations, respectively. Since the clot is always in a state of mechanical equilibrium, we have

$$\frac{\partial \boldsymbol{\sigma_{ij}}}{\partial \boldsymbol{x_j}} = 0\,. \quad (6)$$

As the platelets contract, the clot moves to a different state of mechanical equilibrium, in which the gel deforms and the plasma in the clot will no longer be in chemical equilibrium with the surroundings. Therefore, the gradient of the chemical potential of plasma, drives flow in the clots: $\boldsymbol{J} = -k\nabla\mu/\eta_{sol}\Omega^2$. The conservation of mass dictates

$$\frac{\partial C}{\partial t} = -\nabla \cdot \boldsymbol{J} = \frac{k}{\eta_{sol}\Omega^2}\nabla^2\mu, \quad (7)$$

where k is the permeability of the clot, η_{sol} is the viscosity of the solvent (plasma), respectively.

Initial conditions

The initial clot is in the reference state,

$$\boldsymbol{\sigma}(\boldsymbol{X},0)=0, \quad \mu(\boldsymbol{X},0)=0. \tag{8}$$

Boundary condition for unconstrained contraction

The clot surface is always traction-free and in equilibrium with the surrounding fluid,

$$\boldsymbol{\sigma}(\boldsymbol{X},t)=0, \quad \mu(\boldsymbol{X},t)=0. \tag{9}$$

Boundary condition for constrained contraction

Since the lateral size (20mm) of the blood clot is much larger than the thickness $(400\mu\text{m})$ and the volume is kept unchanged, we assume that all the surfaces are fixed in the constrained contractions by ignoring the boundary effects. Therefore, the clot surface is fixed and in equilibrium with the surrounding fluid,

$$\boldsymbol{x}(\boldsymbol{X},t)=\boldsymbol{X}, \quad J=-\frac{k}{\eta_{sol}\Omega^2}\nabla\mu(\boldsymbol{X},t)=0 \tag{10}$$

B. Mechanical properties of forming blood clots

Recent experimental and computational study shows that the mechanical rigidity increases as fibrin network forms or matures, and the time-dependent stiffness can be described by this relation *(5)*,

$$\frac{K_p}{K_p^m}=\frac{G_p}{G_p^m}=\frac{K_s}{K_s^m}=\frac{G_s}{G_s^m}=\chi(t)=\left(1-e^{-\frac{t}{t_0}}\right)^2, \tag{11}$$

where K_p^m and G_p^m is the bulk and shear modulus of the clotted parallel element, respectively, and K_s^m and G_s^m is the bulk and shear modulus of the clotted series element,

respectively. $\chi(t)$ is the time-dependent relative concentration of fibrin network. t_0 is the characteristic time for the formation of fibrin network, which can be estimated as 500 sec for 3 mg/ml fibrinogen *(5)*. Similar to the stiffness of the fibrin network in Supplemental equation 11, the stall stress and viscosity of platelets are proportional to the concentration of fibrin network,

$$\frac{\sigma_{stall}}{\sigma_s^m} = \frac{\eta_a}{\eta_a^m} = \chi(t), \tag{12}$$

where σ_s^m and η_a^m are the stall stress and viscosity of platelets for matured platelets, respectively.

The recent experiments show the attachment and spreading of adherent cells on microplates take 100-200 sec *(2, 6)*. We further consider the time-dependent formation of stall stress in platelets, which follows the formation of the fibrin network. For simplicity, we assume that the ratio of the current and maximum levels of stall stress has the same function with that of fibrin network formation,

$$\sigma_s^m = S_s^m \left(1 - e^{-\frac{t}{t_1}}\right)^2, \tag{13}$$

where S_s^m is the maximum stall stress of activated platelets. Note that we assume that $t_1 = t_0$ since the attachment and spreading time of adherent cells (100-200 sec) has the same order as the formation time of fibrin network (about 500 sec).

C. Spherically symmetrical active-poroelastic model

For simplicity, we assume the clot is spherical in shape and that the distribution of fibrin network, the platelets and erythrocytes are spherically symmetric. The mechanical and chemical states of the clot are characterized by the radial and hoop stresses, (σ_r, σ_θ), the

concentration, C, and the chemical potential, μ. The deformation of the clot is then described by the radial displacement field, $u(R,t)$, which depends on the radial distance from the center of the clot in the initial configuration, R and time, t. The spherically symmetrical deformation gradients can be expressed as

$$\boldsymbol{F} = \boldsymbol{F_w} = \begin{pmatrix} \lambda_r & 0 & 0 \\ 0 & \lambda_\theta & 0 \\ 0 & 0 & \lambda_\theta \end{pmatrix} = \begin{pmatrix} 1+\partial u/\partial R & 0 & 0 \\ 0 & 1+u/R & 0 \\ 0 & 0 & 1+u/R \end{pmatrix}, \tag{14}$$

$$\boldsymbol{F_a} = \boldsymbol{F_p} = \begin{pmatrix} \lambda_r^a & 0 & 0 \\ 0 & \lambda_\theta^a & 0 \\ 0 & 0 & \lambda_\theta^a \end{pmatrix}, \ \boldsymbol{F_s} = \begin{pmatrix} \lambda_r^s & 0 & 0 \\ 0 & \lambda_\theta^s & 0 \\ 0 & 0 & \lambda_\theta^s \end{pmatrix},$$

where $\lambda_r(R,t), \lambda_\theta(R,t)$ are the radial and hoop stretches, respectively.

Substituting Supplemental equation 14 into Supplemental equation 1, the geometrical relations can be rewritten as

$$\lambda_r = 1 + \frac{\partial u}{\partial R} = \lambda_r^a \lambda_r^s, \qquad \lambda_\theta = 1 + \frac{u}{R} = \lambda_\theta^a \lambda_\theta^s. \tag{15}$$

Substituting Supplemental equation 14 into Supplemental equations 2-5, we get the radial and hoop stress,

$$\sigma_r = K_s \frac{\ln J_s}{J_s} + \frac{2G_s}{3{J_s}^{5/3}}((\lambda_r^s)^2 - (\lambda_\theta^s)^2) - \frac{\mu}{\Omega}, \tag{16}$$

$$\sigma_\theta = K_s \frac{\ln J_s}{J_s} + \frac{G_s}{3{J_s}^{5/3}}((\lambda_\theta^s)^2 - (\lambda_r^s)^2) - \frac{\mu}{\Omega},$$

$$K_s \frac{\ln J_s}{J_s} + \frac{2G_s}{3{J_s}^{5/3}}((\lambda_r^s)^2 - (\lambda_\theta^s)^2)$$

$$= \frac{\sigma_s}{{J_a}^{2/3}} + \eta_a \frac{1}{\lambda_r^a}\frac{\partial \lambda_r^a}{\partial t} + K_p \frac{\ln J_a}{J_a} + \frac{2G_p}{3{J_a}^{5/3}}((\lambda_r^a)^2 - (\lambda_\theta^a)^2),$$

$$K_s \frac{\ln J_s}{J_s} + \frac{G}{3{J_s}^{5/3}}((\lambda_\theta^s)^2 - (\lambda_r^s)^2)$$

$$= \frac{\sigma_s}{{J_a}^{2/3}} + \eta_a \frac{1}{\lambda_\theta^a}\frac{\partial \lambda_\theta^a}{\partial t} + K_p \frac{\ln J_a}{J_a} + \frac{G_p}{3{J_a}^{5/3}}((\lambda_\theta^a)^2 - (\lambda_r^a)^2),$$

where $J_p = \lambda_r^p(\lambda_\theta^p)^2$, $J_s = \lambda_r^s(\lambda_\theta^s)^2$, and $J = (1 + \partial u/\partial R)(1 + u/R)^2$ are the Jacobians representing the relative volume change.

Combining equations. 6, 7, and 14, we can get further the spherically symmetric force balance and plasma diffusion,

$$\frac{\partial \sigma_r}{\partial r} + \frac{2}{r}(\sigma_r - \sigma_\theta) = 0, \tag{17}$$

$$\frac{\partial}{\partial t}(J) = \frac{k}{\eta_{sol}}\frac{1}{r^2}\frac{\partial}{\partial r}\left(r^2 \frac{\partial}{\partial r}\left(\frac{\mu}{\Omega}\right)\right),$$

where $r(R,t) = R + u(R,t)$ is the radial distance from the center of the clot in the current configuration.

Initial conditions

The initial clot is in the reference state,

$$\sigma_r(R,t) = 0, \qquad \sigma_\theta(R,t) = 0, \qquad \mu(R,0) = 0. \tag{18}$$

Boundary conditions for unconstrained contraction

If the initial radius of the clot is denoted by a, the clot surface is always traction-free and in equilibrium with the surrounding fluid,

$$u(0,t) = 0, \qquad J(0,t) = -\frac{k}{\eta_{sol}\Omega^2}\frac{\partial}{\partial r}\big(\mu(0,t)\big) = 0, \tag{19}$$

$$\sigma_r(a,t) = 0, \qquad \mu(a,t) = 0.$$

Boundary conditions for constrained contraction

The clot surface is fixed and in equilibrium with the surrounding fluid,

$$u(0,t)=0, \qquad J(0,t)=-\frac{k}{\eta_{sol}\Omega^2}\frac{\partial}{\partial r}\big(\mu(0,t)\big)=0 \tag{20}$$

$$u(a,t)=0, \qquad \mu(a,t)=0$$

$\sigma_r(r,t), \sigma_\theta(r,t), u(r,t), \mu(r,t)$ can be solved numerically from these partial differential Supplemental equations (Supplemental equations 15-17) with initial condition (Supplemental equation 18) and boundary condition (Supplemental equation 19 or 20) using Mathematica software.

D. Poroelastic and active limits

Now we consider two limits for the spherically symmetrical active-poroelastic model: poroelastic limit ($\eta_{sol}a^2/\eta_a k \gg 1$) and active limit ($\eta_{sol}a^2/\eta_a k \ll 1$), shown in Supplemental Fig. 2.

By fitting the computed degree of contraction vs time curves (Fig. 3 in main text) to actual experimental results, we are able to quantify all of the parameters in our constitutive model under these two limits. The details of the fitting method can be found in section E.

We estimated these parameters: the minimum dimension sample size $a = 1mm$, the viscosity of plasma (mostly water up to 95% by volume) at room temperature $\eta_{sol} = 1.002\, mPa.s$, the permeability $k = 120 \times 10^3 \mu m^2$ for fibrinogen with a concentration of 3mg/ml (1), the active viscosity of these samples $\eta_a = 22.5kPa.s$ (the estimation

details are in section E). The scaled characteristic size can be estimated as $\eta_{sol}a^2/k\eta_a = 4 \times 10^{-7}$, which indicates the activation limit is dominant in the dynamics of contraction for the current sample size. Both the poroelastic and active viscoelastic models fit the unconstrained experimental data well (Supplemental Fig. 3). However, the experiments show that there is no size effect on the unconstrained contraction of a blood clot (Fig. 2 in main text), which is consistent with the activation limit. The permeability of fibrin is dependent on fibrinogen concentration (or deformation), which may result in a transition to the poroelastic limit. Now we estimate the effective fibrinogen concentration of the contracted clot based on the initial fibrinogen concentration and maximum volumetric change. The permeability of fibrin is $k = 7 \times 10^3 \mu m^2$ (1). The scaled characteristic size can be estimated as 7×10^{-6}, which indicates the dynamics of contraction for the current sample size is in the activation limit.

E. Contraction dynamics of maturing blood clot for activation limit

For the activation limit ($\eta_{sol}a^2/k\eta_a \ll 1$), the active-poroelastic model (Supplemental Fig. 1) is the same as the three-element model in the main text (Fig. 3c in the main text), and the stress and deformation relations in

these elements, Supplemental equations 1-2, are rewritten as

$$\boldsymbol{F} = \boldsymbol{F_s F_a} = \boldsymbol{F_s F_p}, \tag{21}$$

$$\boldsymbol{\sigma} = \boldsymbol{\sigma_a}(\boldsymbol{F_a}) + \boldsymbol{\sigma_p}(\boldsymbol{F_p}) = \boldsymbol{\sigma_s}(\boldsymbol{F_s}).$$

The constitutive equations (Supplemental equations 3, 4, 21), the equilibrium condition (Supplemental equation 6), the initial conditions (Supplemental equation 8) and the boundary conditions (Supplemental equations 9 or 10) constitute a well-posed initial

value problem. Since the solution is homogeneous and isotropic, the stresses and deformation gradients can be expressed as $\sigma(t)\boldsymbol{I}$, $\sigma_a(t)\boldsymbol{I}$, $\sigma_p(t)\boldsymbol{I}$, $\sigma_s(t)\boldsymbol{I}$, $\lambda(t)\boldsymbol{I}$, $\lambda_a(t)\boldsymbol{I}$, $\lambda_p(t)\boldsymbol{I}$, and $\lambda_s(t)\boldsymbol{I}$.

Therefore, the governing equations (Supplemental equations 3, 4, 6, 21) can be rewritten by using the time-dependent mechanical properties (Supplemental equations 11-13),

$$\sigma = \sigma_a + \sigma_p = \sigma_s, \qquad J = J_s J_a, \tag{22}$$

$$\sigma_a = \left(\frac{S_s^m}{J_a^{2/3}}\left(1 - e^{-\frac{t}{t_0}}\right)^2 + \frac{\eta_a^m}{3J_a}\frac{dJ_a}{dt}\right)\left(1 - e^{-\frac{t}{t_0}}\right)^2,$$

$$\sigma_p = K_p^m\left(1 - e^{-\frac{t}{t_0}}\right)^2 \frac{\ln(J_a)}{J_a}, \qquad \sigma_s = K_s^m\left(1 - e^{-\frac{t}{t_0}}\right)^2 \frac{\ln(J_s)}{J_s},$$

where $J = \lambda^3$, $J_a = \lambda_a^3$, $J_s = \lambda_s^3$ are the Jacobians representing the relative volume change.

The initial condition (Supplemental equation 8) for homogenous and isotropic deformation can rewritten as

$$J(0) = 1. \tag{23}$$

Unconstrained contraction

The boundary condition (Supplemental equations 9) for homogenous and isotropic deformation can be rewritten as

$$\sigma(t) = 0. \tag{24}$$

Therefore, the governing equations (Supplemental equation 22) can be expressed as

$$J^{1/3}\left(1 - e^{-\frac{t}{t_0}}\right)^2 + \frac{1}{3}\frac{\eta_a^m}{S_s^m}\frac{dJ_a}{dt} + \frac{K_p^m}{S_s^m}\ln(J) = 0, \tag{25}$$

where K_p^m/S_s^m, η_a^m/S_s^m, and t_0 can be determined by fitting the computed clot size , $J^{2/3}$ vs time (t) curves to actual experimental results, shown in Fig. 5a in the main text.

For $t \gg t_0$, the scaled equilibrium Jacobian can be derived from Supplemental equation 25

$$\frac{K_p^m}{S_s^m}\ln(J) + J^{1/3} = 0. \quad (26)$$

We find that the relative clot size , $J^{2/3}$, increases with increasing scaled parallel stiffness, K_p^m/S_s^m, shown in Fig 5a.

For small deformation, the volumetric strain $\varepsilon_v = J - 1 \ll 1$ can be simplified using Supplemental equation 26,

$$\varepsilon_v = -\frac{S_s^m}{K_p^m} \quad (27)$$

Constrained contraction

The boundary condition (Supplemental equation 9) for homogenous and isotropic deformation can be rewritten as

$$J(t) = 1 \quad (28)$$

Therefore, the governing equations (Supplemental equation 22) can be expressed as

$$\frac{\sigma}{S_s^m}\frac{1}{\left(1-e^{-\frac{t}{t_0}}\right)^2} = \left[\frac{1}{J_a^{2/3}}\left(1-e^{-\frac{t}{t_0}}\right)^2 + \frac{1}{3J_a}\frac{\eta_a^m}{S_s^m}\frac{dJ_a}{dt} + \frac{K_s^m}{S_s^m}\frac{\ln(J_a)}{J_a}\right] = -\frac{K_s^m}{S_s^m}\ln(J_a)\,J_a \quad (29)$$

where S_s^m and K_s^m/S_s^m can be determined by fitting the computed total stress (σ), vs time (t) curves to actual experimental results, shown in Fig. 5b in the main text.

For $t \gg t_0$, the scaled equilibrium stress can be derived from Supplemental equation 29,

$$\frac{\sigma}{S_s^m} = \left[\frac{1}{J_a^{2/3}} + \frac{K_p^m}{S_s^m}\frac{\ln(J_a)}{J_a}\right] = -\frac{K_s^m}{S_s^m}\ln(J_a)J_a \qquad (30)$$

We find that the scaled equilibrium stress, σ/S_s^m, decreases with increasing scaled parallel stiffness, K_p^m/S_s^m, and increases with increasing scaled series stiffness, K_s^m/S_s^m, shown in Fig 5b.

For small deformation $\varepsilon_v = J - 1 \ll 1$, the total stress σ can simplified using Supplemental equation 30.

$$\sigma = \frac{S_s^m}{1 + \frac{K_p^m}{K_s^m}} \qquad (31)$$

F. Fitting curves using a random search algorithm

We assume that $S_s^m, \eta_a^m, t_0, K_p^m(0)$, $K_p^m(40\%)$, $K_s^m(0)$, $K_s^m(40\%)$ are the same for different samples under constrained and unconstrained contraction, where 0 and 40% are the concentrations of red blood cells. By fitting the computed degree of contraction and contractile stress vs time curves (Fig. 3 main text) to actual experimental results using a random search algorithm*(7)*, we are able to quantify all of the parameters in our constitutive model in Supplemental Table 1. For each group of parameters, the simulation curves were generated and compared with the experimental data. The optimized parameters were obtained by minimizing the sum of squared residuals (defined as the difference between the experimental and simulation data).

G. The active viscoelastic model with active-series element

The model was simplified to focus on the underlying physics; however, the full model can be found below. The fibrin network is either under tension due to the contraction of platelets (iii or iv), or compression to balance the contractile force generated by the platelets (ii). The stretched fibrin (i and iii) is either directly connected to platelets (iv), or located between the small bundles (which consist of platelets and compressed fibrin) (iii), which can be modeled by an active-series element and series element, respectively. Note that the mechanical response of the active element (i) is the same as that of a dashpot, as it arises from the Hill relation for the platelet. All the passive elements (ii, iii, iv) are generally viscoelastic and solvent migration (v) is also considered in the full model.

The governing equations for this full model (Supplemental equation 22) can be written as,

$$\sigma = \sigma_a + \sigma_p = \sigma_{as} + \sigma_p = \sigma_s, \qquad J = J_s J_p = J_s J_{sa} J_a, \tag{32}$$

$$\sigma_a = \left(\frac{S_s^m}{J_a^{2/3}}\left(1 - e^{-\frac{t}{t_0}}\right)^2 + \frac{\eta_a^m}{3J_a}\frac{dJ_a}{dt}\right)\left(1 - e^{-\frac{t}{t_0}}\right)^2,$$

$$\sigma_{as} = K_{as}^m \left(1 - e^{-\frac{t}{t_0}}\right)^2 \frac{\ln(J_{as})}{J_{as}}$$

$$\sigma_p = K_p^m \left(1 - e^{-\frac{t}{t_0}}\right)^2 \frac{\ln(J_p)}{J_p}, \qquad \sigma_s = K_s^m \left(1 - e^{-\frac{t}{t_0}}\right)^2 \frac{\ln(J_s)}{J_s},$$

Here the subscript sa denotes the active-series element. K_{as}^m, J_{as}, and σ_{as} represent the bulk modulus, stress, and Jacobian of the active-series element.

For unconstrained contraction:

$$J_a^{\frac{1}{3}}\left(1 - e^{-\frac{t}{t_0}}\right)^2 + \frac{1}{3}\frac{\eta_a^m}{S_s^m}\frac{dJ_a}{dt} + \frac{K_p^m}{S_s^m}\frac{J_a}{J}\ln(J) = 0 \tag{33}$$

$$\ln J = \frac{K_{as}^m}{K_p^m + K_{as}^m J_a}\ln(J_a) J_a$$

For constrained contraction:

$$\frac{\sigma}{S_s^m}\frac{1}{\left(1-e^{-\frac{t}{t_0}}\right)^2}=\left(\frac{1}{J_a^{2/3}}\left(1-e^{-\frac{t}{t_0}}\right)^2+\frac{1}{3J_a}\frac{\eta_a^m}{S_s^m}\frac{dJ_a}{dt}\right)+\frac{K_p^m}{S_s^m}\frac{\ln(J_p)}{J_p}$$

$$=-\frac{K_s^m}{S_s^m}\ln(J_p)J_p \qquad (34)$$

$$K_p^m\ln(J_p)+K_{as}^m\ln(J_p/J_a)J_a=-K_s^m\ln(J_p)(J_p)^2$$

There is no significant difference between for the simulation results using the full model and the simplified model for both unconstrained and constrained contraction. Here the fitted bulk modulus of active series element is $K_{as}^m=16S_s^m=7.2kPa$. This conclusion is consistent with the fact that the elastic modulus of platelets is ~10kPa (2), which is much higher than that of the fibrin network, which has an elastic modulus below 1kPa (3, 4). Therefore, we can further simplify the full model to the 3-element model by assuming that the active-series stiffness is infinite. Furthermore, if there is no series element (iii) in our model, the normal stress will be same for the constrained clot with or without the RBCs (Supplemental Fig. 6). From both the electron microscopy image (Supplemental Fig. 7a) and experimental measurement (Supplemental Fig. 8), we can conclude that the active-series element is not necessary while the fibrin-RBC series element should be included.

H. Viscoelasticity of fibrin and RBCs

Fibrin only behaves in a viscoelastic manner at high strain rates but remains elastic at low strain rates due to the fact that the loss modulus of fibrin, G'', is dependent on the strain rate while the storage modulus, G', is not. For the oscillation tests completed by Kim et al (4), the frequency used is $f=0.5-10Hz$ and strain amplitude is $\varepsilon=0.005-0.03$, so the strain rate is estimated as $\dot{\varepsilon}=4\varepsilon f=0.01-0.12s^{-1}$. The strain rate for free contraction in our manuscript can be estimated as $\dot{\varepsilon}=0.8/3/1000=0.0004s^{-1}$ based

on an area change of 0.8 and time scale of 1000s. The strain rate for our experiments is much smaller than that of the oscillation tests completed by Kim et al (4), as such it is reasonable to treat fibrin as an elastic material. In the oscillation tests by van Kempen et al (3), the loss modulus is at least 2 orders smaller than G' for the frequency of 1-3Hz and the amplitude 0.01 (strain rate 0.04 to $0.12s^{-1}$). This is again consistent with the conclusion that G'' is negligible compared to G' for the low strain rate used in our manuscript, confirming that fibrin will behave as an elastic material rather than a viscoelastic one.

The viscosity of blood, μ_R, at room temperature can be estimated at 10 times that of water, around $10.02\ mPa$. This allows for the viscous stress on RBCS to be calculated as $\sigma_v = \mu_R \dot{\varepsilon} = 1.002 \times 10^{-6}\ Pa$ based on the strain rate in our experiments $\dot{\varepsilon} = 0.0004s^{-1}$. The elastic stress contribution of fibrin network is $\sigma_e = K\varepsilon = 0.4 - 40Pa$, where $K = 1 - 100Pa$ is the stiffness range of fibrin network and $\varepsilon = 0.4$ is the strain amplitude in our experiment. The RBCs and fibrin networks are in parallel in our model, thus we can directly compare the viscous stress on RBCs (σ_v) and elastic stress on fibrin network (σ_e), and conclude that the viscous contribution of RBCs is negligible and can be treated as an elastic material.

The full active viscoelastic poroelastic model including an active, active-series, parallel, and series element is shown in Supplemental Fig. 9. 1) The poroelastic element, 2) the active-series element, and 3) the viscoelasticity of parallel and series element can be ignored to obtain the current 3-element model for the following reasons:

a) The poroelastic element: As the sample size, a, is comparable to the intrinsic length of a material, $(k\eta_a/\eta_{sol})^{1/2}$, the viscoelasticity and poroelasticity must be considered simultaneously, where η_a is the active coefficient, η_{sol} is the viscosity

of the solvent, k is the permeability of the clot. For small clots $a \ll (k\eta_a/\eta_{sol})^{1/2}$, the contraction dynamics of clot is controlled by active viscoelasticity. (Details in Supplemental methods D)

b) The active-series element: The elastic modulus of platelet is around 10kPa (Lam WA et al, *Nat Mater.* **10**, 61-66 (2011), which is much stiffer than that of the fibrin network which has an elastic modulus below 1kPa (Van Kempen et al., Biophys. J. 107: 504 & Kim et al., Biomaterials. 35: 6739). Furthermore, there is almost no difference between the full model and the simplified models. (Details in Supplemental methods G)

c) The viscoelasticity of the series and parallel elements: Fibrin only behaves in a viscoelastic manner at high strain rates but remains elastic at low strain rates, because the loss modulus of fibrin, G'', is dependent on the strain rate and the storage modulus, G' remains unchanged. In the oscillation tests in Ref. 19, the loss modulus is at least 2 orders of magnitude smaller than G' in the frequency range of 1-3Hz and strain amplitude of 0.01 (strain rate 0.04 to $0.12s^{-1}$). We can conclude that G'' is negligible compared to G' for the low strain rate case considered in our manuscript ($0.0002s^{-1}$); so fibrin will behave as an elastic material rather than viscoelastic. (Details given in Supplemental methods H)

Supplemental Figures

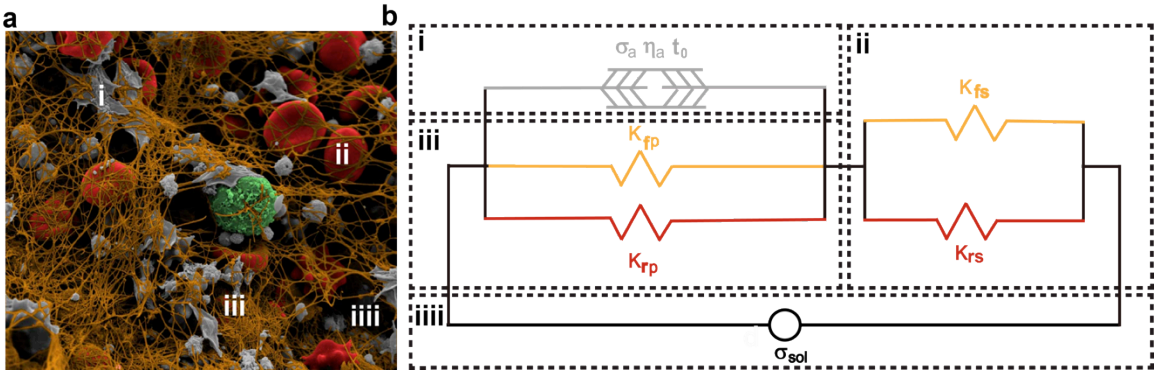

Supplemental Figure 1. An active – poroelastic model for blood clots (a) The whole blood clot is made up of a branched network of fibrin network (tan), platelet aggregates (gray), and RBCs (red). (b) The active-poroelastic model consists of two passive elastic elements to represent the elasticity of the series (ii) and parallel (iii) elements, an active contractile element (i), and a porous element (iiii).

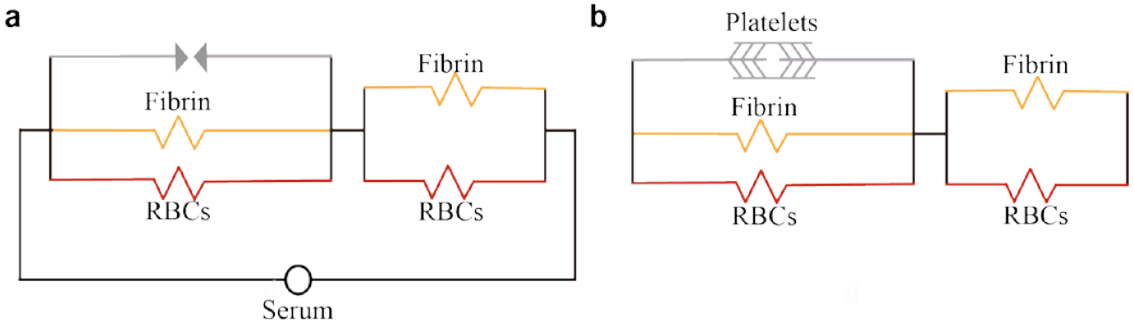

Supplemental Figure 2. Poroelastic and active limit of contraction. (a) poroelastic limit as $\eta_{sol}a^2/k\eta_a \gg 1$. (b) active limit for $\eta_{sol}a^2/k\eta_a \ll 1$.

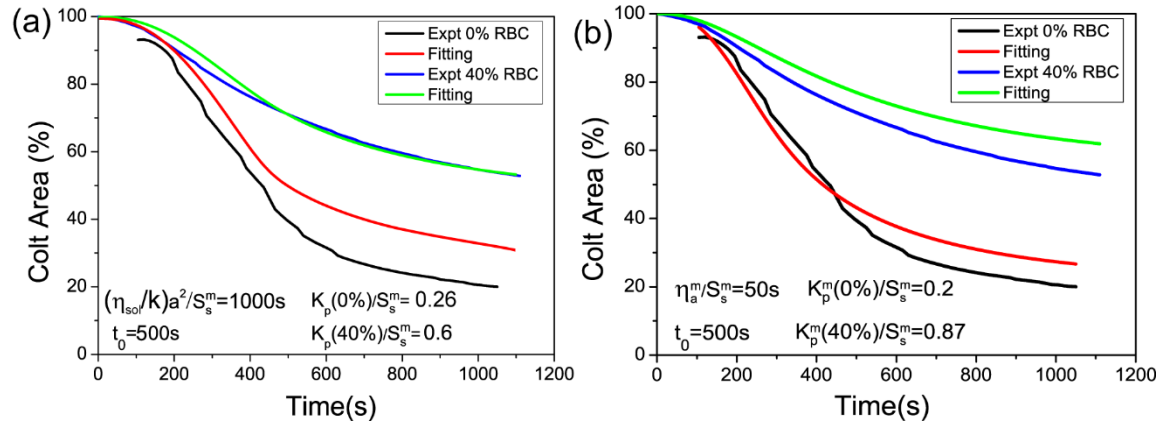

Supplemental Figure 3. Poroelastic and active viscoelastic model. The unconstrained contraction for (a) the poroelastic limit: $\eta_{sol}a^2/k\eta_a \gg 1$, and for (b) the active limit: $\eta_{sol}a^2/k\eta_a \gg 1$. For simplicity, we assume that $K_s \gg K_p$ and $G_p/K_p = 3(1-2\nu_p)/2(1+\nu_p)$, where the initial Poisson's ratio $\nu_p = 0.3$ for the poroelastic limit.

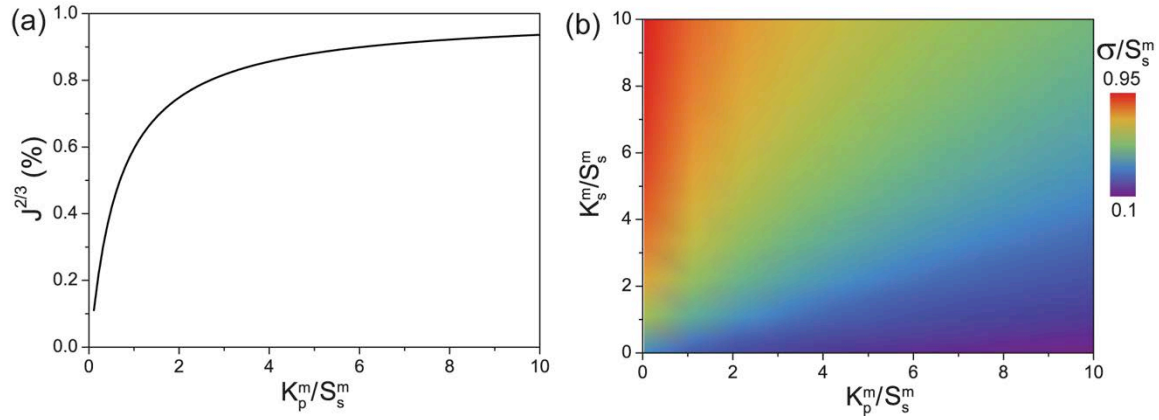

Supplemental Figure 4. The influence of scaled parallel and series stiffnesses (K_p^m/S_s^m and K_s^m/S_s^m, respectively) on degree of unconstrained contraction ($J^{2/3}$) and stress of constrained contraction (σ/S_s^m) for $t \gg t_0$. (a) Equilibrium $J^{2/3}$ versus K_p^m/S_s^m. (b) Contour plots of equilibrium σ/S_s^m as a function of K_p^m/S_s^m and K_s^m/S_s^m. Colors (blue to red) represent σ/S_s^m (0.1–0.95).

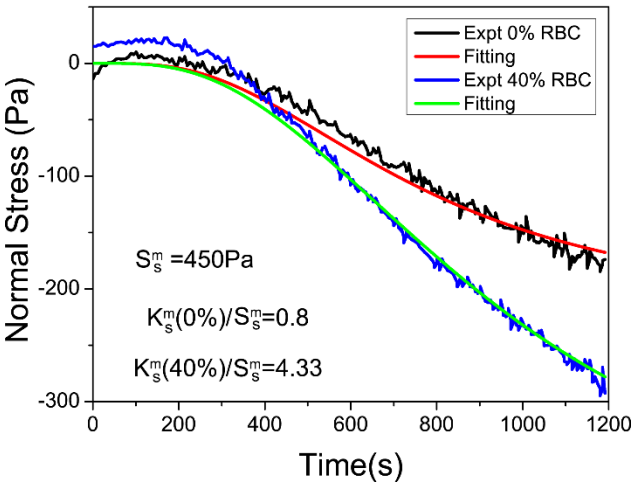

Supplemental Figure 5. Simulation of stall stress. Contractile stress was modeled to extend until stall stress was reached for samples with RBCs (green) and samples without RBCs (red).

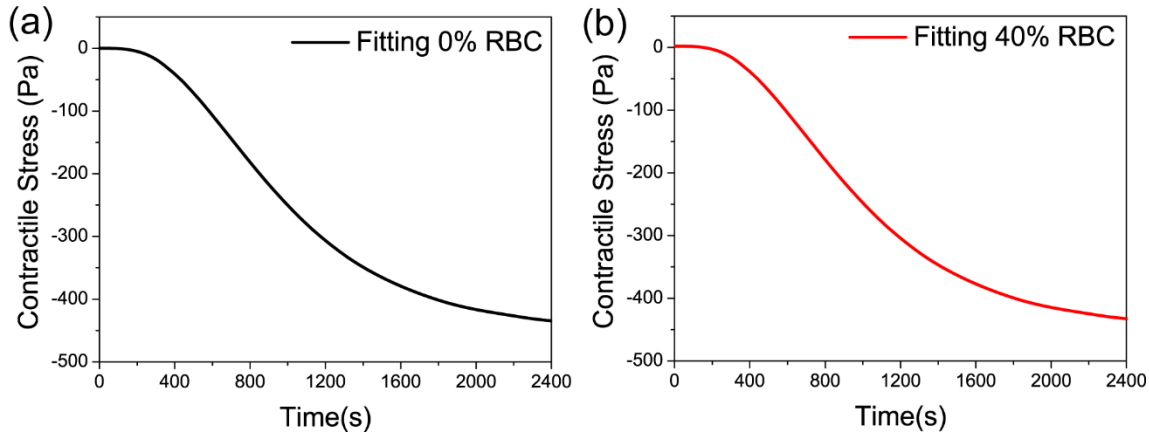

Supplemental Figure 6. Contractile stress in the absence of a series element. Contractile stress was simulated for samples without and with RBCs (black and red lines, respectively) without series element ($K_s^m(0\%) \to \infty, K_s^m(40\%) \to \infty$).

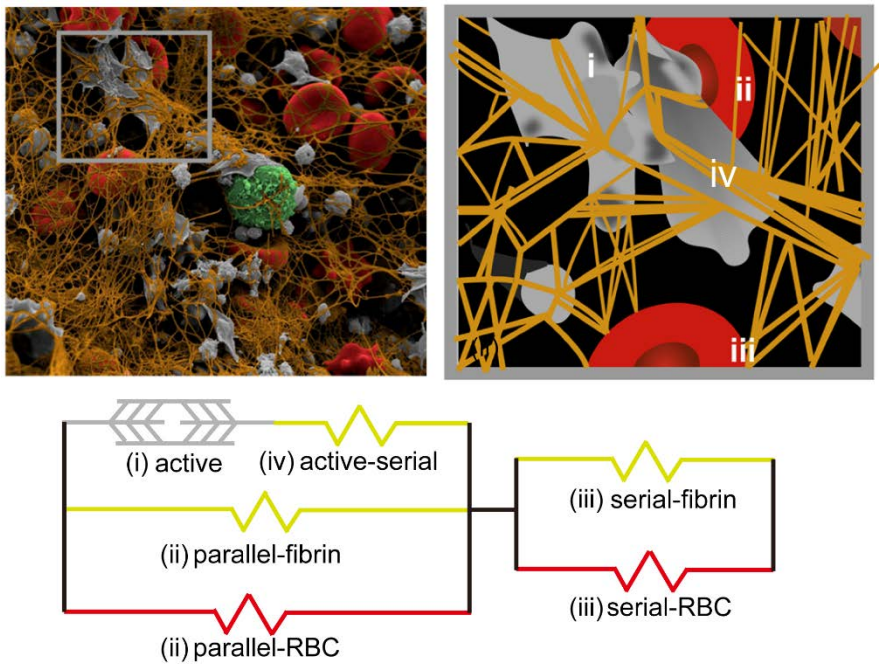

Supplemental Figure 7. The full active viscoelastic model with active, active-series, parallel, and series element.

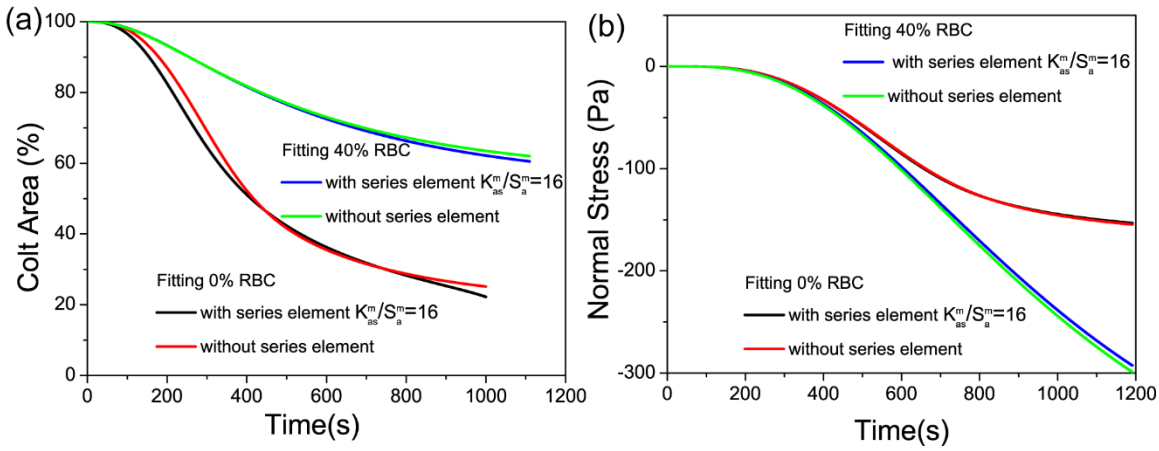

Supplemental Figure 8. Comparison of unconstrained (a) and constrained (b) clot contraction using the full model with the active–series element (solid lines) and the simplified 3-element model (dashed lines). The fitted active-series stiffness the provides the best fit is $K_{as}^m = 16S_s^m = 7.2kPa$.

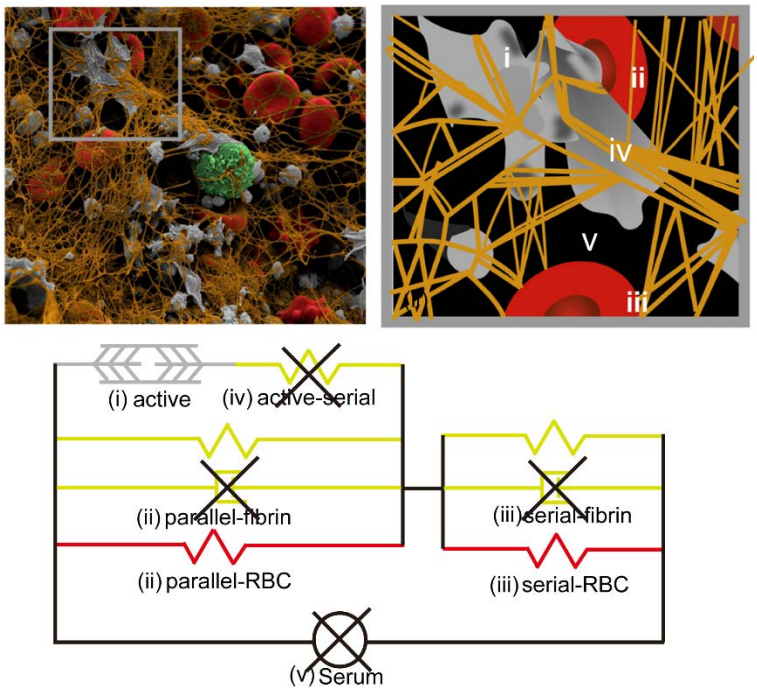

Supplemental Figure 9. The full active visco-poro-elastic poroelastic with active, active-series, parallel, serial, and serum element. The active-series element, the serum element, the viscoelasticity of parallel element, the viscoelasticity of parallel element can be ignored to obtain the current 3-element model.

Supplemental Table 1. Comparison of fitting parameters to known literature values

	Stall stress $S_s^m(Pa)$	Active viscosity $\eta_a^m/S_s^m(s)$	Time delay $t_0(s)$	Parallel stiffness $K_p^m(0\%)$	Parallel stiffness $K_p^m(40\%)$	Series stiffness $K_s^m(0\%)$	Series stiffness $K_s^m(40\%)$
Fitting	450	50	500	90	392	360	1948
Experimental estimation	270 (2)	250 (2)	500 (3)	$1-100$ (4)		500 (3)	

1. Wufsus, A.R., N.E. MacEra, and K.B. Neeves. 2013. The hydraulic permeability of blood clots as a function of fibrin and platelet density. Biophys. J. 104: 1812–1823.
2. Lam, W.A., O. Chaudhuri, A. Crow, K.D. Webster, T.-D. Li, A. Kita, J. Huang, and D.A. Fletcher. 2011. Mechanics and contraction dynamics of single platelets and implications for clot stiffening. Nat. Mater. 10: 61–66.
3. Van Kempen, T.H.S., A.C.B. Bogaerds, G.W.M. Peters, and F.N. Van De Vosse. 2014. A constitutive model for a maturing fibrin network. Biophys. J. 107: 504–513.
4. Kim, O. V., R.I. Litvinov, J.W. Weisel, and M.S. Alber. 2014. Structural basis for the nonlinear mechanics of fibrin networks under compression. Biomaterials. 35: 6739–6749.